0.1 E06-014

Precision Measurement of d_2^n: Probing the Lorentz Color Force

S. Choi, X. Jiang, Z.-E. Meziani, B. Sawatzky, spokespersons,
and
the d_2^n and Hall A Collaborations.
contributed by D. Parno, D. Flay and M. Posik.

0.1.1 The Experiment

Experiment E06014 ran in Hall A from February 7 to March 17, 2009, at production beam energies of 4.73 and 5.89 GeV, on a polarized ^{3}He target. The LHRS and BigBite were deployed as independent detectors, each oriented at an angle of 45° to the beamline. Each detector effectively operated as a single-arm experiment, with the LHRS measuring the unpolarized scattering cross section and BigBite measuring double-spin asymmetries in scattering between a longitudinally polarized electron beam and longitudinally and transversely polarized ^{3}He gas. The experiment was designed to provide extensive coverage of the deep inelastic scattering region, over ranges of $0.2 \leq x \leq 0.7$ and $2\ \text{GeV}^2 \leq Q^2 \leq 6\ \text{GeV}^2$.

This experiment ran immediately after E06010, which used a similar configuration, and some calibration runs were shared between the two experiments. E06014 was the commissioning experiment for a gas Čerenkov detector in the BigBite stack, as well as for a new photon detector and integrating data-acquisition system for the Compton polarimeter. Beamline calibrations have been completed, and detector calibrations are well underway.

Measurement of d_2^n The primary purpose of E06014 is the measurement of the quantity d_2^n, a probe of the strong force formed by taking the second moment of a linear combination of the unpolarized structure functions g_1 and g_2, as follows:

$$d_2^n\left(Q^2\right) = \int_0^1 x^2 \left[2g_1^n\left(x, Q^2\right) + 3g_2^n\left(x, Q^2\right)\right] dx \tag{1}$$

In addition to the access it gives to quark-gluon correlations through its dependence on g_2^n, d_2^n is of physical interest in its own right. A precision measurement of this quantity can be used to test lattice QCD predictions. At low values of Q^2, d_2^n can be associated with spin polarizabilities within the nucleon [1]. At high values of Q^2, d_2^n is best interpreted as a measure of the transverse color Lorentz force on a struck quark, averaged over the nucleon as a whole [1, 2].

E06-014 sought to accomplish the measurement of d_2^n in the deep inelastic scattering region by combining measurements of three quantities. With the LHRS, we took data for the measurement of the unpolarized total cross section σ_0. In BigBite, we took data for measuring two asymmetries formed between opposite target-beam spin configurations: $A_\parallel$, formed when both beam and target are polarized longitudinally, and $A_\perp$, formed when the target is polarized transverse to the longitudinal beam polarization. $A_\parallel$ and $A_\perp$ are typically measured as asymmetries in the counting rates for each spin configuration:

$$A_\parallel = \frac{N^{\downarrow\Uparrow} - N^{\uparrow\Uparrow}}{N^{\downarrow\Uparrow} + N^{\uparrow\Uparrow}} \quad \text{and} \quad A_\perp = \frac{N^{\downarrow\Rightarrow} - N^{\uparrow\Rightarrow}}{N^{\downarrow\Rightarrow} + N^{\uparrow\Rightarrow}}$$

Our independent measurements of σ_0, $A_\parallel$ and $A_\perp$ may then be combined into a measurement of d_2^n:

$$d_2^n = \int_0^1 \frac{MQ^2}{4\alpha^2} \frac{x^2y^2}{(1-y)(2-y)} \sigma_0 \left[\left(3\frac{1+(1-y)\cos\theta}{(1-y)\sin\theta} + \frac{4}{y}\tan\left(\theta/2\right)\right) A_\perp + \left(\frac{4}{y} - 3\right) A_\parallel\right] dx \tag{2}$$

where we have made use of the kinematic variables $x = Q^2/2M\nu$ (the Bjorken x variable), $\nu = E - E'$ (the energy transfer from electron to target), θ (the scattering angle of the electron), and $y = \nu E$ (the fractional energy transfer from electron to target). This expression of d_2^n, in terms of directly measurable quantities rather than structure functions, allowed us to divide our allocated beam time so as to minimize the error on the d_2^n measurement itself, rather than the error on the measurements of g_1 and g_2. Our expectation is that

the E06014 measurement will represent a fourfold improvement in precision from previous world data [3], in advance of an approved 12 GeV experiment in Hall C that should push the precision and kinematic range still higher [4].

Measurement of A_1^n The data taken for the d_2^n measurement will also allow us to measure the longitudinal neutron-virtual photon asymmetry A_1^n. When the nucleon and the virtual photon it exchanges with a lepton are both longitudinally polarized, the cross section of the process can be denoted $\sigma_{1/2(3/2)}$, where the subscript gives the projection of the total spin along the virtual photon's momentum direction when the spins are anti-parallel (parallel). A_1 is then defined as:

$$A_1\left(x,Q^2\right) \equiv \frac{\sigma_{1/2}-\sigma_{3/2}}{\sigma_{1/2}+\sigma_{3/2}} \approx \frac{g_1\left(x,Q^2\right)}{F_1\left(x,Q^2\right)} \text{for high } Q^2 \tag{3}$$

We may also express A_1 in terms of the parallel and perpendicular asymmetries $A_\parallel$ and $A_\perp$:

$$A_1 = \frac{1}{D\left(1+\eta\xi\right)}A_\parallel - \frac{\eta}{d\left(1+\eta\xi\right)}A_\perp \tag{4}$$

where D is the virtual photon polarization factor and η, ξ, and d are quantities set by kinematics and by the virtual photon polarization vector.

Measuring A_1^n on an effective polarized neutron target (such as ^{3}He), when combined with measurements of A_1^p on a polarized proton target, gives access to the polarized-to-unpolarized parton distribution function ratios $\Delta u/u$ and $\Delta d/d$. Recent results from Hall A [5, 6] and from CLAS [7] showed a significant deviation of $\Delta d/d$ from the predictions of perturbative QCD, which have that ratio approaching 1 in the limit of $x \to 1$ (Figure 1). As part of the 12 GeV program, two approved experiments (one in Hall A [8] and one in Hall C [9]) will extend the accuracy and x range of this measurement, but a measurement of A_1^n at E06-014's kinematics will provide valuable support (or refutation) of prior Jefferson Lab results, while producing additional input for theoretical models in advance of the coming experiments at 12 GeV. Figure 2 shows existing world A_1^n data, as well as the projected statistical errors for the E06014 measurement using a 5.9 GeV beam. (Statistical errors for the measurement at $E_e = 4.7$ GeV are not shown.)

0.1.2 Analysis Progress: Left HRS

Data from the Left HRS will be used to compute the total unpolarized cross section σ_0, which will contribute to our measurement of d_2^n. Here, we discuss our analysis progress on Left HRS data over the past year. In addition to the major points discussed below, we have confirmed that the E06010 optics are suitable for the needs of this experiment, and have begun to study data quality over our six weeks of running.

Particle Identification Particle identification (PID) in the Left HRS relies primarily on the gas Čerenkov and pion rejectors, whose efficiencies must be known to high precision in order to measure a cross section. Fortunately, the two detectors may be used to calibrate one another.

Figure 3 shows the gas Čerenkov ADC sum, in photoelectrons, at a typical kinematic setting. The blue histogram contains events labeled as pions by the pion rejector, while the red histogram contains events labeled as electrons. (The black spectrum is the sum of the two.) If a cut is placed at two photoelectrons (magenta line), 96% of electrons are kept with a pion rejection factor f of about 600 pions per electron. These results are typical across the whole kinematic range.

The results of a pion rejector PID study are shown in Figure 4. Here, the pions (blue) and electrons (red) are selected according to readings in the gas Čerenkov. These distributions are cleanly separated in E/p: a cut at $E/p = 0.54$, corresponding to the magenta line, accepts 99% of electrons while giving a pion rejection factor of about 680 pions per electron.

The combined rejection factor from both detectors is expected to be on the order of at least 10^4 pions per electron.

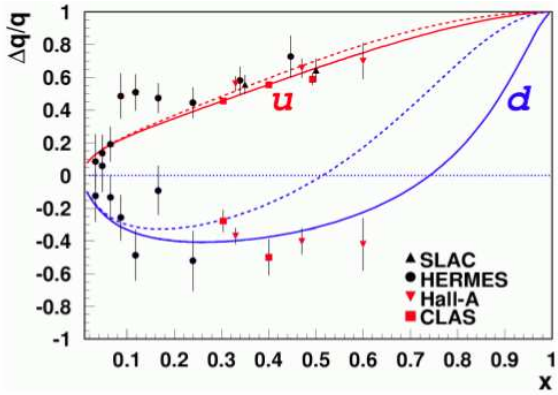

Figure 1: $\Delta q/q$ as a function of x, reproduced from PR12-06-110 [9]. Dashed lines show the predictions of LSS(BBS) parameterizations, which use leading-order perturbative QCD with hadron helicity conservation [10]. Solid lines show predictions that explicitly include a nonzero term for the orbital angular momentum of valence quarks [11].

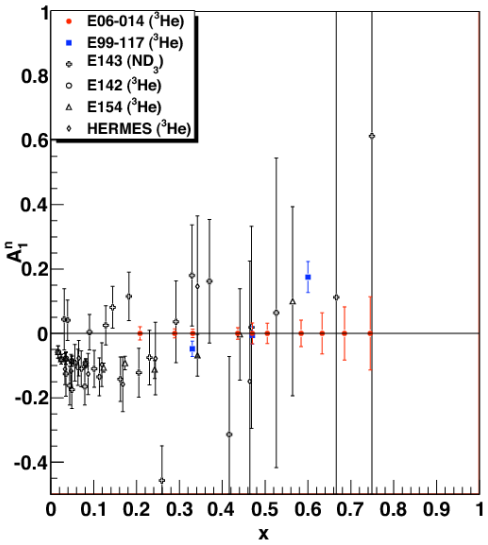

Figure 2: Projected statistical errors for E06-014's A_1^n measurement with five-pass beam are shown in red, along with results from previous experiments [6, 12, 13, 14, 15, 16]. Bins are chosen to match the acceptance of the LHRS kinematic settings for the d_2^n measurement.

Trigger Efficiency The primary Left HRS trigger for E06-014 was the T3 trigger, formed by requiring a hit in both the S1 and S2m scintillator planes; in effect, this requires that one paddle in each scintillator plane record a hit on both its left and its right. The T4 trigger, formed by requiring a hit in two out of three detectors (the S1 scintillator plane, the S2m scintillator plane, and the gas Čerenkov, excluding an S1-S2m coincidence), allows a check on the T3 efficiency.

In order to determine the T3 trigger efficiency, we start from the equation:

$$\varepsilon_{T3} = \frac{N_{T3}}{N_{T3} + N_{T4}}, \tag{5}$$

where $N_{T3(4)}$ is the number of T3(4)-type events adjusted for prescaling, defined as follows:

$$N_{T3(4)} = ps_{T3(4)} \times \mathrm{bit}_{T3(4)}, \tag{6}$$

where $ps_{T3(4)}$ is the prescale value for the T3(4) trigger and $\mathrm{bit}_{T3(4)}$ is the number of times the bit pattern was set – that is, the number of events that passed the prescale condition. The reason for using this definition for $N_{T3(4)}$ is to avoid a possible situation where, for instance, some T4 triggers do *not* pass the prescale condition. This would imply (based on Equation 5) that the T3 trigger efficiency is better than it actually is.

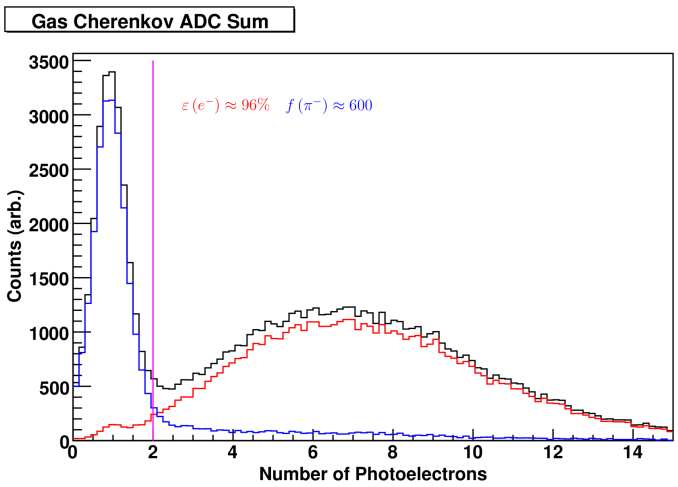

Figure 3: PID efficiency of LHRS gas Čerenkov. Pions are shown in blue and electrons in red, as determined by the pion rejectors. The magenta line shows the location of the proposed gas Čerenkov pion rejection cut.

Table 1 shows the results binned by LHRS momentum setting. The trigger efficiency proved to be better than 99.9% across the whole kinematic range.

p (GeV)	E (GeV)	ε_{T3} (%)	ε_1 (%)
1.23	1.23	99.99	98.981 ± 0.192
0.60	4.73	99.95	99.282 ± 0.592
0.60	5.89	99.96	99.339 ± 0.430
0.80	4.73	99.93	99.209 ± 0.843
0.90	5.89	99.95	99.293 ± 0.796
1.13	5.89	99.93	99.228 ± 1.037
1.20	5.89	99.98	99.213 ± 1.307
1.27	5.89	99.94	99.172 ± 0.967
1.42	4.73	99.95	99.189 ± 1.235
1.42	5.89	99.93	98.810 ± 1.176
1.51	4.73	99.92	99.104 ± 1.149
1.51	5.89	99.96	99.172 ± 1.326
1.60	4.73	99.96	98.953 ± 1.421
1.60	5.89	99.96	98.832 ± 1.413
1.70	5.89	99.96	98.620 ± 1.924

Table 1: The T3 trigger efficiency ε_{T3} and the VDC one-track efficiency ε_1 for each LHRS kinematic setting.

VDC One-Track Efficiency The inefficiency of the VDCs (Vertical Drift Chambers) arises due to mistakes in the software computation of tracks, usually as a result of multi-track events or no-track events. In multi-track events, many particles cross the VDC planes simultaneously, resulting in a large number of possible trajectories. Therefore, we retain only one-track events in our analysis of the various physics quantities of interest; however, we need to be aware that such a requirement will discard any good tracks that arrive in multi-track events. To understand the effect of the one-track event requirement, we examine the zero-, multi-, and one-track efficiencies, taking zero- and multi-track efficiencies as the *inefficiency* of the VDC tracking algorithm [17].

We define the *one-track efficiency* as follows: we count the number of one-track events and compare this sum to the sum of all zero-, one-, and multi-track events. Mathematically, we have:

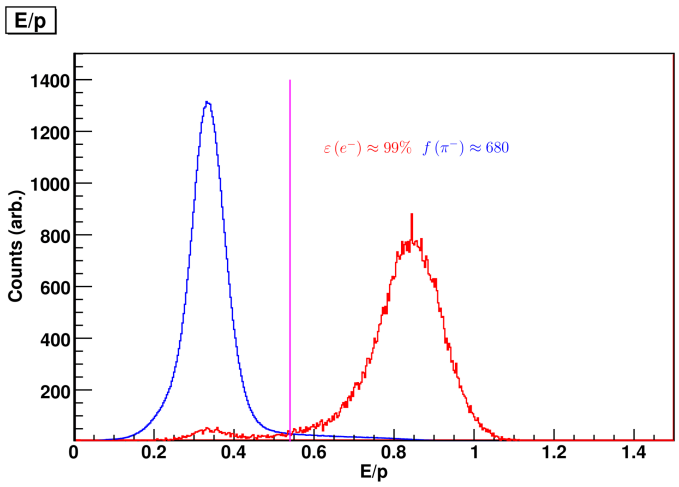

Figure 4: PID efficiency of LHRS pion rejectors. The pion E/p spectrum is shown in blue and the electron spectrum in red, as determined by the gas Čerenkov. The magenta line shows the location of the proposed pion rejector cut.

$$\varepsilon_1 = \frac{N_1}{\sum_{i=0}^{4} N_i}, \tag{7}$$

where N_1 is the number of one-track events, and N_i is the number of i-track events ($i = 0, \ldots, 4$). (The software reconstructs a maximum of up to four tracks per event [18, 19].) Similarly, we may determine the other j-track efficiencies ($j \neq 1$) as:

$$\varepsilon_j = \frac{N_j}{\sum_{i=0}^{4} N_i}. \tag{8}$$

We measured one-track efficiencies ε_1 in excess of 99% across our entire kinematic range, as shown in Table 1.

0.1.3 Analysis Progress: BigBite

Data from BigBite will be used to compute the parallel and perpendicular asymmetries $A_\parallel$ and $A_\perp$, which will contribute to our measurement of d_2^n and to our measurement of A_1^n. Since BigBite is not being used to measure a cross section, absolute efficiencies are somewhat less important than they are for the Left HRS. Here, we discuss our analysis progress on BigBite data over the past year. In addition to the topics described in detail below, we have begun to study data quality and compute preliminary asymmetries.

MWDCs An analysis of track residuals has been completed for several runs; residuals for all planes range from 190 to 265 microns. Figure 5 shows representative residual plots for the six u planes.

Optics We took as a starting point the BigBite optics package for E06010 [20], which allowed us to rapidly achieve an excellent vertex reconstruction (Figure 6) with centimeter-level resolution.

For our momentum reconstruction, we deviated from the E06010 approach, adapting its first-order optics model and adding a correction factor at low momenta in order to correctly place the $\Delta(1232)$ peak in our one-pass, elastic H_2 calibration data. With $p^{(1)}$ the adapted first-order momentum, the final reconstructed momentum p is of the form

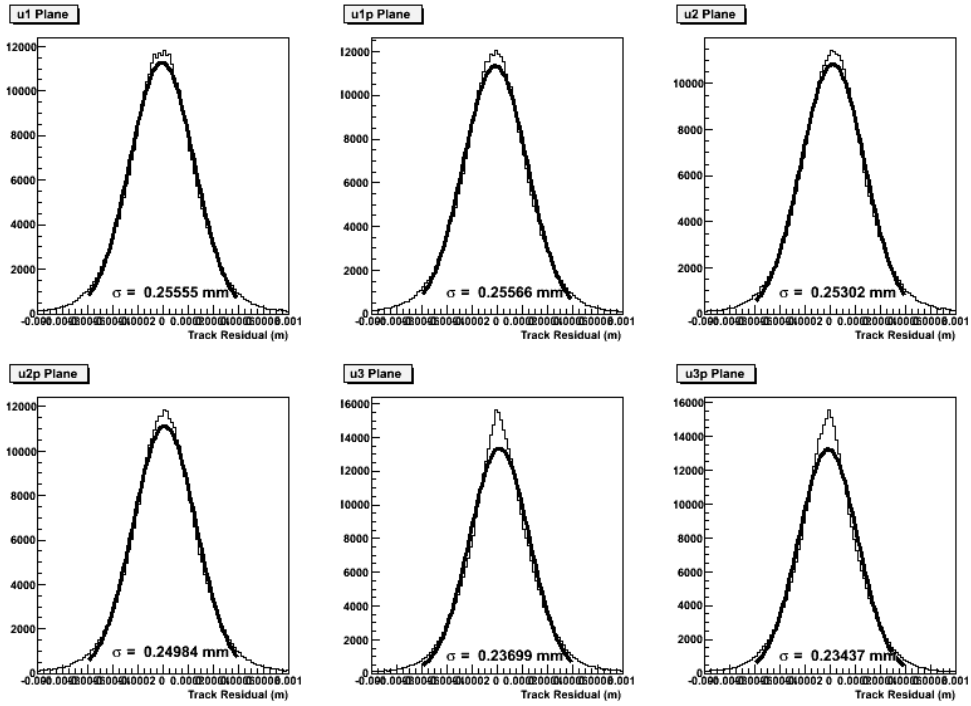

Figure 5: Track residuals for u planes in the multi-wire drift chambers.

$$p = \begin{cases} p^{(1)} & \text{for } p^{(1)} > 0.95 \text{ GeV} \\ p^{(1)} - 3.7\left(p^{(1)} - 0.95\text{GeV}\right)^2 & \text{for } 0.85 \leq p^{(1)} \leq 0.95 \text{ GeV} \\ p^{(1)} + 0.148\left(p^{(1)} - 0.9\text{GeV}\right) & \text{for } p^{(1)} < 0.9 \text{ GeV} \end{cases} \quad (9)$$

The form of this correction was chosen to ensure continuity in the final momentum spectrum. Figure 7 shows the resulting invariant mass spectrum for elastic scattering from hydrogen atoms. Figure 8 shows a momentum resolution of 1.07% for the same data.

Gas Čerenkov E06014 was the commissioning experiment for the BigBite gas Čerenkov, which was placed in the detector stack between the multi-wire drift chambers and the preshower. This device proved to be an excellent tool for removing pion contamination, both in the online trigger and in offline analysis. Figure 9 shows the ADC signal spectra in the gas Čerenkov for pions (in blue) and for electrons (in red), for both high-rate and low-rate parts of the detector.

Shower ■☞Eagerly awaiting final calibration to insert in this space!

0.1.4 Analysis Progress: Target

Yawei Zhang, for the Target Group, has completed preliminary analysis of the target data, including internal temperature and density values and calibration of NMR results to EPR measurements. Figure 10 shows the resulting preliminary target polarization numbers, run by run. Few NMR measurements were taken in the time around Run 20400, since the experiment was taking a few days of unpolarized beam at that point; the paucity of data leads to an anomalously low extrapolated polarization there.

References

[1] M. Burkardt. *hep-ph/0905.4079v1.*

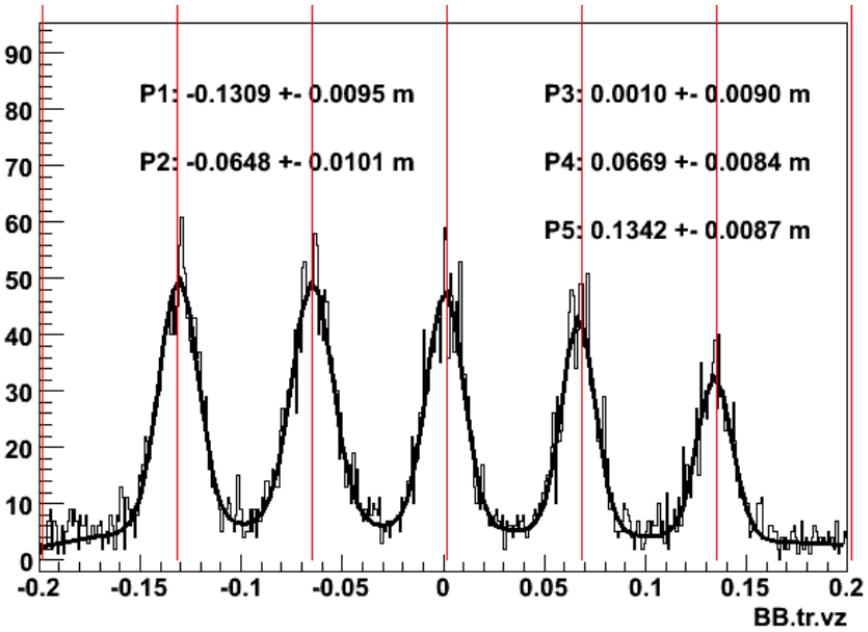

Figure 6: Vertex reconstruction for tracks belonging to negatively-charged particles issuing from a carbon-foil target in a five-pass run. The measured peak locations are compared to the surveyed foil positions, marked in red.

[2] M. Burkardt. *hep-ph/0902.0163v1.*

[3] S. Choi, Z.-E. Meziani, X Jiang, B. Sawatzky, et al. *Jefferson Lab PAC PR-06-014*, 2005.

[4] T. Averett, W. Korsch, Z.-E. Meziani, B. Sawatzky, et al. *Jefferson Lab PAC E1206121*, 2010.

[5] X. Zheng et al. *Phys. Rev. Lett.*, 92:012004, 2004.

[6] X. Zheng et al. *Phys. Rev. C*, 70:065207, 2004.

[7] K. V. Dharmawardane et al. *Phys. Lett. B*, 641:11, 2006.

[8] G. Cates, N. Liyanage, Z.-E. Meziani, G. Rosner, B. Wojtsekhowski, X. Zheng, et al. *Jefferson Lab PAC E1206122*, 2006.

[9] G. Cates, J.-P. Chen, Z.-E. Meziani, X. Zheng, et al. *Jefferson Lab PAC E1210101*, 2010.

[10] E. Leader, A. V. Sidorov, and D. B. Stamenov. *Int. J. Mod. Phys.*, A13:5573, 1998.

[11] H. Avakian, S.J. Brodsky, A. Deur, and F. Yuan. *Phys. Rev. Lett.*, 99:082001, 2007.

[12] D. Adams et al. *Phys. Lett. B*, 357:248, 1995.

[13] P. L. Anthony et al. *Phys. Rev. D*, 54:6620, 1996.

[14] K. Ackerstaff et al. *Phys. Lett. B*, 404:383, 1997.

[15] K. Abe et al. *Phys. Rev. Lett.*, 79:26, 1997.

[16] K. Abe et al. *Phys. Rev. D*, 58:112003, 1998.

[17] P. H. Solvignon. PhD thesis, Temple University, August 2006.

[18] J. Alcorn et al. *Nucl. Instr. and Meth. in Phys. Res. A*, 522:294, 2004.

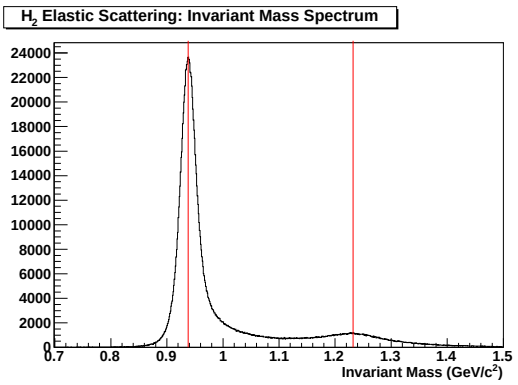

Figure 7: Reconstructed invariant mass spectrum for H_2 elastics data in BigBite. The red lines mark the known masses of the proton and of the $\Delta(1232)$.

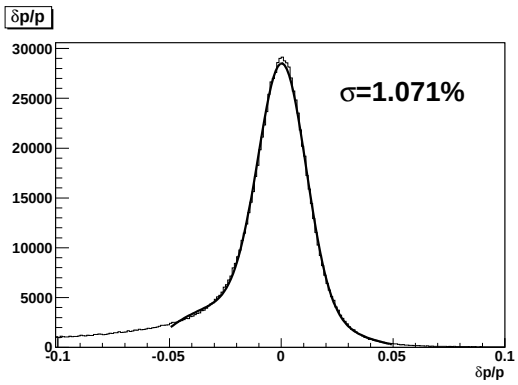

Figure 8: Momentum resolution for BigBite negative optics, plotted as $\delta p/p = (p - p_{elas})/p$.

[19] A. Orsborn. Report for DoE Science Undergraduate Laboratory Internship Program, 2005.

[20] X. Qian. PhD thesis, Duke University, May 2010.

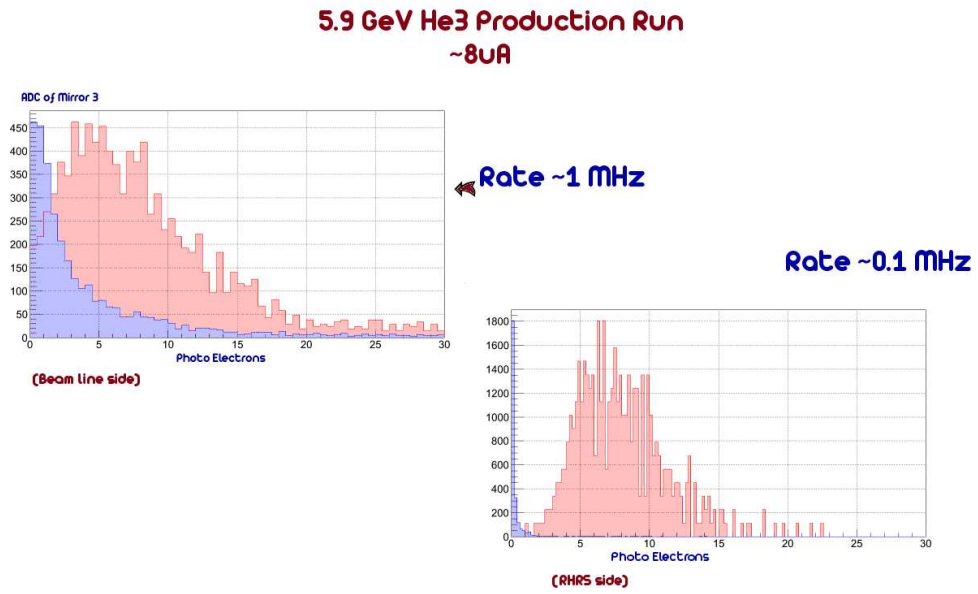

Figure 9: ADC signals in selected PMTs of the BigBite gas Čerenkov for pions (blue) and electrons (red). The near-beam side of the detector (left) sees a rate about ten times higher than the far-from-beam side (right).

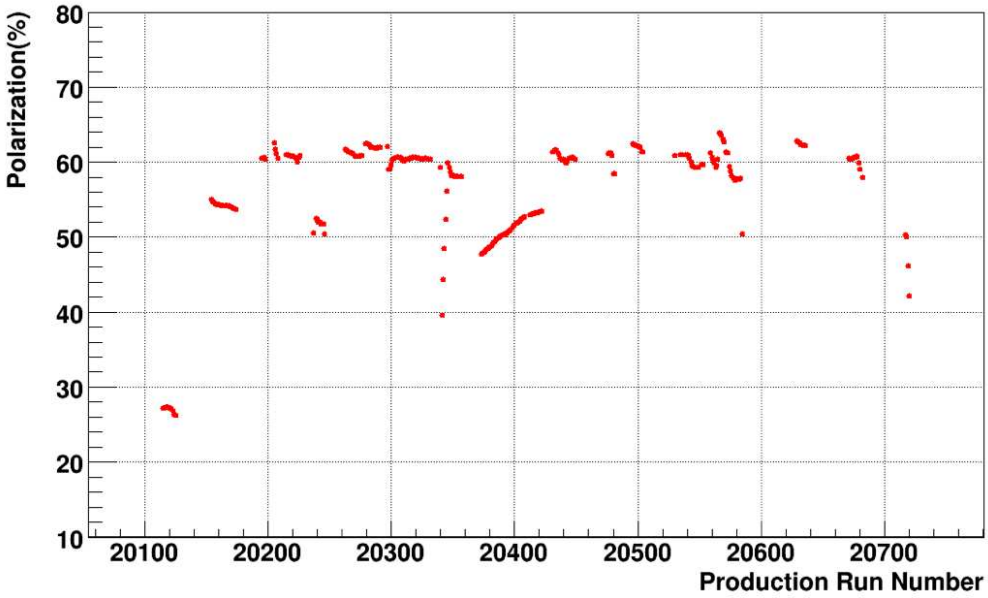

Figure 10: Preliminary run-by-run target polarizations for E06014, based on NMR and EPR measurements. The low-polarization region centered on Run 20400 represents an unreliable extrapolation from only a few data points.